IEEE Access
Multidisciplinary | Rapid Review | Open Access Journal

Received 30 March 2024, accepted 23 April 2024, date of publication 30 April 2024, date of current version 15 May 2024.

Digital Object Identifier 10.1109/ACCESS.2024.3395468

RESEARCH ARTICLE

Bidirectional Support for Individual Finger Joints in Soft Rehabilitation Gloves: Integration of Foldable Pouch Actuators With Modular Elastomeric Actuators

SHOTA KOKUBU[1], PABLO E. TORTÓS VINOCOUR[1], AND WENWEI YU[1,2], (Member, IEEE)
[1]Graduate School of Science and Engineering, Chiba University, Chiba 263-8522, Japan
[2]Center for Frontier Medical Engineering, Chiba University, Chiba 263-8522, Japan

Corresponding author: Wenwei Yu (yuwill@faculty.chiba-u.jp)

This work was supported in part by the Japanese Society for the Promotion of Science (JSPS) KAKENHI under Grant JP23KJ0307.

ABSTRACT In recent years, a proliferation of soft actuators tailored for hand rehabilitation has been observed. In particular, modular soft actuators have garnered particular interest due to their capacity for individual customization and joint-specific support, a feature often lacking in whole-finger soft actuators. Despite these advancements, a significant limitation persists: the majority of these actuators facilitate only finger flexion, neglecting the equally vital extension movements required for comprehensive hand rehabilitation. Traditional approaches to achieving multi-degree-of-freedom or bidirectional motion have relied on the integration of multiple chambers within soft actuators. However, this strategy has proven impractical for modular soft actuators, primarily due to spatial constraints within the finger joint. To address this challenge, we introduce a foldable pouch actuator (FPA). Designed as a flat, foldable structure composed of a single sheet, the FPA expands solely upon pressurization, generating the requisite force for finger extension. Notably, the FPA seamlessly integrates with existing modular soft actuators without compromising their structural integrity or functional capabilities, thereby enabling bidirectional support for individual joints. Evaluations using a synthetic finger model achieved a joint flexion torque of 0.17 Nm and estimated an overall extension torque of 0.12 Nm. These advancements were accomplished without compromising the traditional flexion functionality, adding individual joint extension support to the existing capabilities. This study constitutes a substantive leap forward in the utilization of soft actuators for clinical hand rehabilitation applications.

INDEX TERMS Soft robotics, soft actuator, hand rehabilitation, finger-motion assistance, active extension support, bidirectional support.

I. INTRODUCTION

In the field of hand rehabilitation, soft rehabilitation gloves have recently gained significant traction. Particularly noteworthy is the emergence of soft pneumatic actuators crafted from elastomeric materials, which have found extensive application in rehabilitation gloves [1], [2], [3], [4]. Owing to their inherent viscoelastic properties, these elastomeric materials confer safety, biocompatibility, and portability upon the actuators. Moreover, the pneumatic nature of these actuators renders them advantageous for hand rehabilitation due to their use of uncontaminated driving resources and back-drivability features.

Among various actuator designs, fiber-reinforced elastomer actuators have emerged as a leading technology to facilitate the bending motion of finger joints. These

The associate editor coordinating the review of this manuscript and approving it for publication was Tao Wang.

actuators feature fibers arranged in an asymmetric pattern around the elastomer chambers [5], [6], [7]. This fiber-reinforcement not only directs the bending of the actuators in predetermined paths but also enhances their pressure resistance and bending strength. Empirical studies and mathematical models have corroborated that optimizing the spatial arrangement, number of windings, and winding methods for reinforcement fibers can yield a bending angle commensurate with a patient's specific joint range of motion (ROM) [8], [9].

While initial research efforts have primarily concentrated on the actuation of simple flexion movements for the entire finger, a pressing need remains for joint-specific customization and motion support. Given that patients with paralysis often exhibit limited joint ROM and variable joint stiffness, the imperative for individualized active support in hand rehabilitation is clear [4], [10]. Importantly, these biomechanical constraints can differ even among the joints of a single patient, necessitating a nuanced approach to therapeutic support [11], [12], [13]. Additionally, many patients exhibit joint stiffness at particular angles [14], thereby requiring actuators that can provide bidirectional movement—both flexion and extension—for effective rehabilitation.

Therefore, the advancement of soft actuators for rehabilitation applications necessitates the development of technologies that can be customized to provide active, bidirectional support at individual joints, in line with the specific requirements of real-world rehabilitation scenarios.

The modularization of soft actuators emerges as a promising strategy for achieving individual customization and targeted joint support. Unlike conventional whole-finger soft actuators, modular soft actuators allocate a separate actuator to each joint (top left and middle left of Fig. 1). Various designs, including fabric-based, bellows-based, and fiber-reinforced elastomer-based actuators, have been developed to facilitate individualized adaptations [4], [15], [16], [17], [18]. These modular units, connected through 3D-printed components, offer ease of personalization [17], [18]. Previous studies, including our own, have substantiated the utility of modular actuators in providing support for individual joint motion [17], [18]. Nonetheless, these actuators generally offer only passive extension support—a limitation also observed in other elastomeric actuators—and such support may prove inadequate for patients with contractures [2], [19], [20], [21], [22], [23], [24].

Bellows-based actuators represent an attempt to facilitate bidirectional motion; they achieve this by capitalizing on the expansion and contraction dynamics of the bellows. However, these actuators encounter challenges related to distortion during expansion and suboptimal force generation during flexion, generating forces as low as approximately 1.9 N as reported in [16].

In other words, the majority of module actuators are designed to facilitate only finger flexion and neglect to provide for extension, a critical aspect of hand rehabilitation.

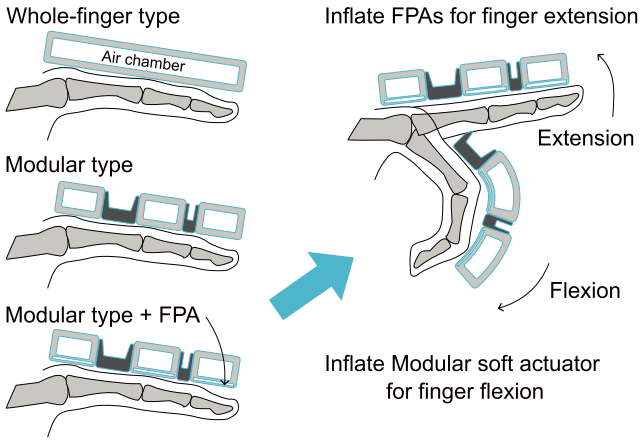

FIGURE 1. Introduction of conventional soft actuator types and concept of bi-directional support of individual hand joints using foldable pouch actuator (FPA).

Even the limited number of actuators capable of bidirectional support fail to offer adequate solutions. To enhance the capabilities of existing modular actuators, one viable solution involves the incorporation of an extension support mechanism specifically designed to complement flexion support. Our previous modular actuators were capable of providing adequate flexion support for individual joints. Although prior research has advocated the use of multi-chambered designs to achieve multiple degrees of freedom and bidirectional motion [6], [25], this approach introduces significant drawbacks. Specifically, multi-chambered configurations result in increased size and often induce mechanical interference among the chambers [26]. Thus, the integration of multiple chambers within the confined dorsal space of a finger presents formidable challenges.

Given these structural limitations, there is a pressing need to develop a new type of actuator that reconciles compactness, force-to-weight ratio, and compatibility as an antagonistic element. This requirement exists alongside the multi-chamber approach, and aims to successfully integrate an extension support mechanism without compromising the flexion capabilities of the existing modular actuators.

In this study, we introduce a foldable pouch actuator (FPA), a novel design specifically engineered for facile integration into existing modular actuators to facilitate finger extension. The pouch actuator distinguishes itself through its flat, lightweight structure while retaining an impressive force-to-weight ratio [27], [28], [29]. Comprising an inflatable, airtight bladder constructed from thermoplastic sheet material, the pouch actuator is capable of converting volumetric changes induced by air pressure into either contraction or rotation. Furthermore, the magnitude of force or stiffness generated is contingent upon the cross-sectional area during the actuator's expansion phase and is customizable through geometric considerations [27], [30]. As such, pouch actuators

hold promise for assisting finger extension by producing the requisite stiffness and can be accommodated in the limited spaces within existing actuators(bottom left and right of Fig. 1).

However, the challenge lies in achieving sufficient stiffness, defined here as an adequate cross-sectional area during the expansion phase, within the spatial constraints of pre-existing actuators. To address this issue, the FPA design incorporates a folding mechanism that allows the cross-sectional area to enlarge only when subjected to air pressure. This folding architecture enables the pouch to expand more robustly under pressure, thereby potentially achieving a larger cross-sectional area and, consequently, greater stiffness than would be attainable with a simpler design. Additionally, upon deflation, the FPA is designed to revert to its original dimensions, thereby precluding any interference with the functioning of the existing actuators.

This study presents the architecture of the FPA and its seamless integration into modular actuators. We characterize these actuators in terms of bending angle, tip force, and load-deflection when operated independently. Additionally, the performance of the integrated actuators is assessed through evaluations of joint ROM and torque during experiments involving a dummy finger. Finally, repetition test of flexion and extension movements and grasping test were performed using soft rehabilitation gloves. The findings from these characterizations and evaluations are comprehensively discussed, culminating in conclusions drawn from the empirical results.

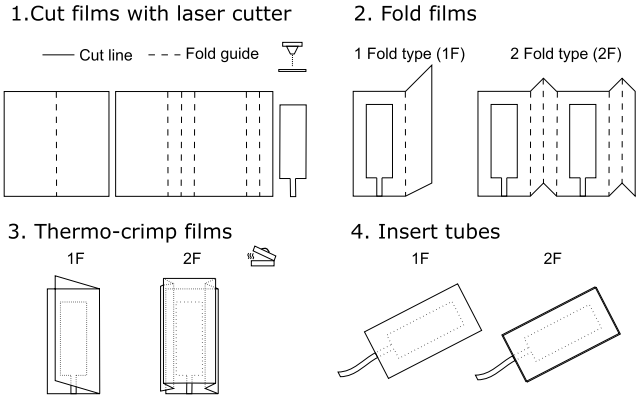

FIGURE 2. Fabricating process of FPA. Each number indicates the order of fabrication. The left side of each illustration indicates the 1F type FPA, and the right side shows the 2F type.

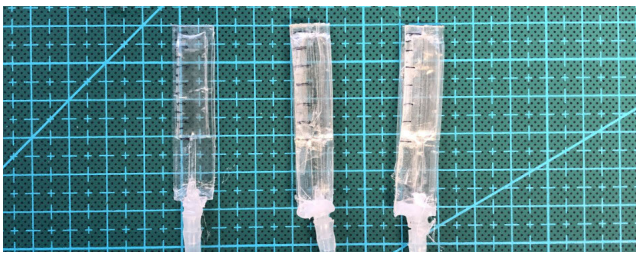

FIGURE 3. Three FPA prototypes. From left to right: 1F, 2F Mid, and 2F Max type.

II. DESIGN AND MODELING

A. FOLDABLE POUCH ACTUATOR (FPA)

In the current study, we engineered a FPA utilizing a thermoplastic film. Notably, the film employed in the construction of the FPA is flexible but lacks elasticity. As a result, the internal chamber formed by the film expands and engenders stiffness exclusively when pressurized, and it reverts to its initial configuration upon depressurization without occupying additional space. This compact nature of the FPA not only renders its integration into existing actuators more straightforward but also streamlines the manufacturing process.

The fundamental architectural principles of the FPA share similarities with several sheet and fabric-based flat pneumatic actuators [31], [32], [33]. An FPA is constructed from two layers of sheets, which are crimped together to form an internal chamber. Positioned on the dorsal side of the finger joints, the FPA stiffens and elongates upon pressurization, thereby generating an extension torque that extends the finger joints. Designed to fit within the restricted dorsal space above each joint, the FPA aims to offer individualized joint support. Nonetheless, this design constraint inherently limits the chamber's volume, potentially compromising the generated extension torque. To mitigate this limitation, the present study employed a folding architecture, as opposed to a simple flat design, to maximize the volume of the pressurized chamber and thereby ensure adequate extension torque, even when the FPA must conform to restricted dimensions.

Fig. 2 depicts the fabrication procedure and prototype specifications in detail. Initially, a developmental blueprint for the FPA was conceived, and the requisite film was precision-cut using a laser cutter. Subsequently, the cut film was manipulated into its folded shape using a dedicated template. To preclude adhesion of the chamber and tube insertion regions during the sealing process, certain areas were masked with tape. A heat sealer was then employed to unite all terminal edges of the folded film through mechanical pressure. Ultimately, a tube was inserted between the unsealed portions of the film, and any potential for air leakage was nullified using an adhesive sealant applied via a glue gun.

FPAs are categorized into two primary types: the 1 Fold (1F) and the 2 Fold (2F), depending on whether a folding structure is incorporated. The 2F category is further subdivided into middle (2F Mid) and maximum (2F Max) types based on the depth of the fold d. In the current investigation, prototypes were constructed using various combinations of chamber length L and folding structures associated with the radius of the expansion chamber R. The aim was to corroborate the performance of these prototypes and their

TABLE 1. Design parameters of FPA. For each type of FPA, design parameters such as fold depth *d* and expected radius of expansion *R* were set differently.

Folding type	Fold depth d	Chamber radius R	Chamber length L
1Fold	0	$8/\pi$	5, 10, 15, 20*
2F Mid	2.25	$12/\pi$	
2F Max	5.5	$16/\pi$	

'$*$' Length L is common to all types (mm)

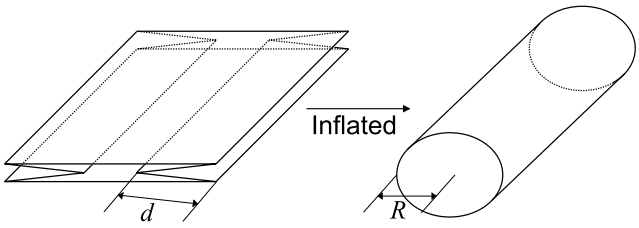

FIGURE 4. Modeling of FPA expansion by air pressure.

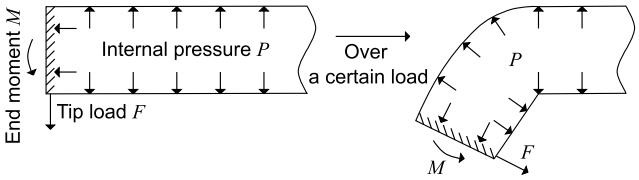

FIGURE 5. Modeling of failures that occur when loads are applied to the tip of the FPA.

alignment with the theoretical model discussed subsequently. The specific design parameters for the FPA are enumerated in Table 1. Three types of prototypes were produced according to each design parameter (Fig. 3). It is important to note that the three types of FPAs are almost identical in appearance and their size. This means that even if the internal structure differs due to the folded structure, they still have the same ease of integration into existing actuators.

Upon inflation, the folded section of the FPA expands, functioning akin to a cylindrical beam, thereby significantly augmenting its stiffness as depicted in Fig. 4. This inflated condition is commonly described as an ''inflatable tube.'' When modeled as a cantilevered beam, its load-bearing capability is understood to be a function of its internal pressure [30]. When subjected to a lateral load, wrinkles begin to appear on the surface of the inflatable tube. The tube reaches its yield point when these wrinkles extend to its outer circumference, as illustrated in Fig. 5.

Main et al. [30] demonstrated that the moment of failure can be succinctly represented by Equation 1:

$$M = \pi P R^3 \tag{1}$$

where P is the internal pressure and R is the radius of the expansion chamber. Additionally, the critical load can be expressed as follows:

$$F = \frac{M}{L} \tag{2}$$

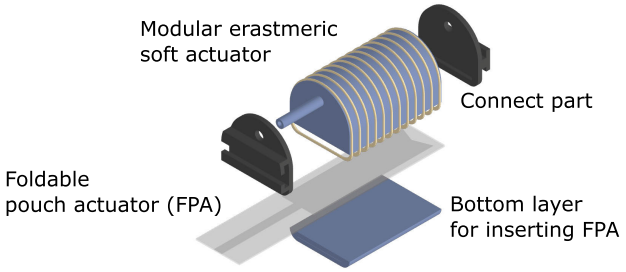

FIGURE 6. Design for integrating FPA into a modular elastomer actuator and the components of the integrated actuator.

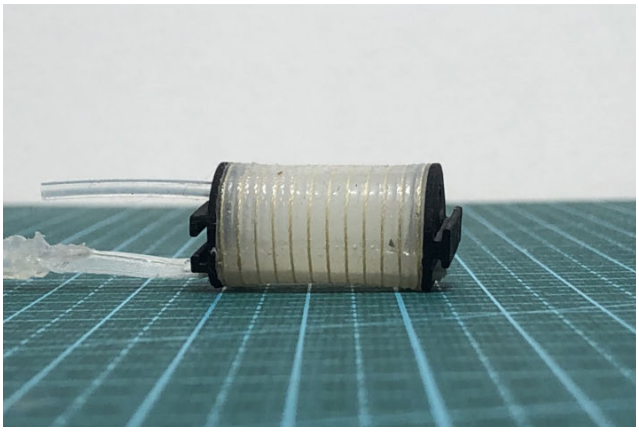

FIGURE 7. Integrated actuator prototype. FPA is inserted in the bottom of the modular elastomer actuator.

The stiffness-induced bending of the FPA at the finger joints is conceptually analogous to the failure of the inflatable tube. Therefore, the maximum load and extension support performance of the FPA are equivalent and can be approximated by Equation 2. Moreover, as indicated in Equation 2, the radius of the expansion chamber plays a crucial role in determining the maximum load because the maximum load is proportional to the third power of the radius. Therefore, it is expected from the model that adding a folding structure effectively improves extension support performance while maintaining the compactness of the FPA.

B. MODULAR SOFT ACTUATOR

For the flexion mechanism, we utilized a pre-existing modular elastomeric soft actuator developed in our previous research [4], [18]. This actuator is specifically engineered to facilitate the flexion of an individual joint. Its chamber asymmetry and fiber reinforcement enable directional bending upon pressurization. The three modular elastomeric soft actuators are interconnected by 3D-printed spacers, which offer support for flexion across all three joints of a single finger. Additionally, the spacer length can be customized to accommodate individual requirements. The sole distinction between the current and the pre-existing model lies in the provision of space at the base of the modular elastomeric soft actuator for the insertion of the FPA, as depicted in Fig. 6.

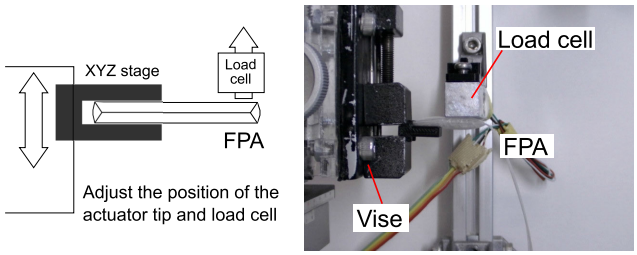

FIGURE 8. Measurement setup with FPA only. Diagram illustrating the maximum load measurement to characterize the FPA, accompanied by a photograph of the equipment.

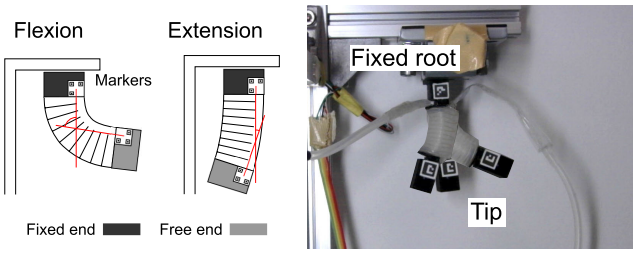

FIGURE 9. Measurement setup with integrated actuator. The diagram shows how the integrated actuator measures bending angles in the flexion and extension directions, accompanied by a photograph of the equipment.

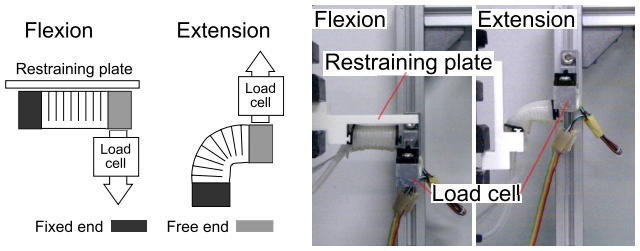

FIGURE 10. Measurement setup with integrated actuator. The diagram and photograph demonstrate that the positioning of the tip force measurement varies with the direction of force generation, namely flexion and extension.

C. INTEGRATED ACTUATOR

In this integrated system, the modular elastomeric soft actuator serves the role of a flexion actuator, while the FPA functions as an extension actuator. The combination of these two actuators can generate both flexion and extension torques, facilitating bidirectional movement of the finger joints. The elastomeric layer surrounding the FPA contributes passive extension torque and allows for rapid deflation and return to its original form upon depressurization. Conversely, an unpressurized FPA restricts the extension of the elastomeric base layer, thus assisting in the bending mechanism during actuation. Actuators were fabricated based on the average dimensions of Japanese index fingers as a reference point (Fig. 7) [34].

III. EXPERIMENTS

A. CHARACTERIZATION OF FOLDABLE POUCH ACTUATOR

The stiffness or force output of the FPA, aimed at assisting finger joint extension, was indirectly evaluated by measuring the maximal load under pressurized conditions. Three sets of experiments were carried out to examine the effects of principal design parameters—namely, length L, radius R, and air pressure P on this maximal load. In these experiments, two parameters were held constant to isolate the variable of interest. The term ''maximum load'' is defined as the peak value of the vertical force exerted on the pressurized FPA when it undergoes bending.

Initially, the FPA was secured to an XYZ stage, with its tip making contact with a load cell (SC133-2kg, Sensor and Control Co., ltd). Starting from this baseline position, the FPA was progressively elevated, and the resulting contact force on the load cell was measured, as illustrated in Fig. 8. The actuator reaches a yielding point around its fixed root when subjected to a load exceeding a certain threshold. Beyond this yielding point, the tip force experiences a substantial reduction. The tip force immediately prior to this yielding event was documented as the maximum load.

B. CHARACTERIZATION OF INTEGRATED ACTUATOR

The integrated actuator is comprised of an FPA and a modular elastomeric actuator. Given the FPA's exceptionally thin architecture, the external appearance of the integrated actuator closely resembles that of a conventional modular elastomeric actuator. Characterization of the integrated actuator was conducted based on metrics such as angular displacement during actuation, the force exerted at the tip, and the stiffness of the flexion and extension chambers when activated concurrently.

Angular displacement is defined through vectors originating at the actuator's tip and root. This angle was quantified using 2D markers affixed to both the tip and root of the actuator; calculations were then performed based on coordinates captured from camera imagery (ELP-USBFHD08S-MFV, Shenzhen Ailipu Technology Co., Ltd), as shown in Fig. 9.

The force generated at the actuator's tip was assessed through a measurement setup incorporating a vise and a load cell to stabilize the actuator, as delineated in Fig. 10. In measurements related to the bending side, a restraining plate was positioned atop the actuator's surface to constrain upward deformation. This approach has been validated in multiple analogous studies and facilitates the measurement of maximal tip force while minimizing nonlinear effects attributable to actuator deformation [6], [31]. Conversely, the tip force concerning the extension aspect was defined as the force needed to straighten the actuator from a pre-bent state and was assessed using a comparable setup. In these experiments, the initial bending angle was set at 90°. Both the modular elastomeric actuator and the FPA were subject to separate pneumatic pressurization.

The stiffness of the integrated actuator was indirectly characterized by the deflection observed in response to the load applied at the actuator's tip, as shown in Fig. 11.

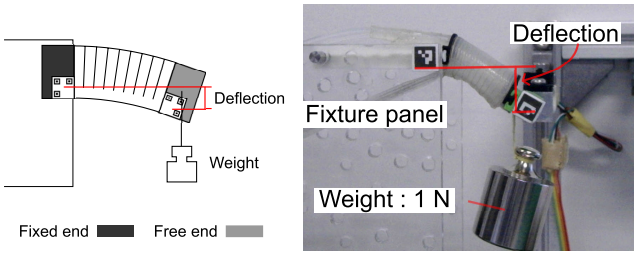

FIGURE 11. Measurement setup with integrated actuator, with a diagram depicting the load deflection measurement process used to characterize the actuator, and a photograph showcasing the actual equipment.

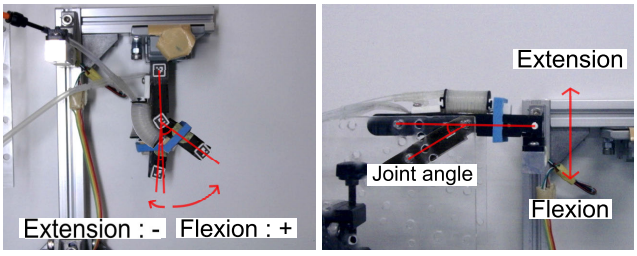

FIGURE 12. Measurement setup with integrated actuator and dummy fingers. Each measurement item is, from left to right, joint range of motion (ROM) and joint torque.

Both flexion and extension chambers were subjected to various combinations of air pressures, resulting in vertical displacement of the tip from its original position. The amount of deflection was determined through analysis of camera images, using 2D markers as reference points.

C. EVALUATION OF ACTUATORS WITH DUMMY FINGER

The effectiveness of the integrated actuator was assessed through a ROM and torque tests performed on a dummy finger. The dummy finger was fabricated based on the average dimensions of Japanese index fingers, as referenced in previous research [34]. The distal interphalangeal (DIP), proximal interphalangeal (PIP), and metacarpophalangeal (MCP) joints were modeled as pin-joint configurations. Individual integrated actuators were placed on each joint and were interconnected using rigid connectors. For measurement purposes, the dummy finger was also equipped with markers to facilitate ROM quantification and a specialized structure for securing it to the measurement platform. Within the scope of these experiments, only the MCP joint's ROM and torque were examined. This focused approach was justified by our previous work, which established identical ROM and torque behaviors across all three finger joints [18].

The ROM was articulated as the angular displacement occurring between the joint's initial and final positions during actuation, as depicted in Fig. 12. ROM values were ascertained using 2D markers attached to the dummy finger's joints, with coordinates captured via camera imagery. The ROM measurement process involved two distinct pressurization sessions: one for the modular elastomeric actuator and another for the FPA.

To quantify joint torque, an experimental setup was employed wherein the dummy finger was immobilized at a specific joint angle, and the force generated at a predetermined distance from the joint was measured, as outlined in Fig. 12. In this configuration, the joint angle could be varied between 0° and 90° in increments of 15°. Joint torque was calculated as the product of the measured force and the distance separating the center of the joint from the load cell's point of contact. Torque measurement was performed in two segments, focusing separately on flexion and extension.

D. SOFT REHABILITATION GLOVE PERFORMANCE

The integrated actuator was adapted for human application through a series of grasping tests facilitated by a specially designed glove-like device. Actuators affixed to the glove were strategically positioned to align with the joints of the subject's finger, thereby enabling assisted movement of each joint. These actuators were tethered to a pneumatic control system, including a regulator (ITV0031-2ML, SMC Corporation), via pneumatic tubing and manipulated through a graphical user interface (GUI).

At first, a repetition test of flexion and extension movements was undertaken, focusing on a glove-assisted hand during its grasping motion. Glove-assisted flexion and extension motion were achieved by pressurizing chambers corresponding to the respective directions of the actuators installed in the glove. The control signals for the flexion and extension chambers' air pressure were modeled as sine curves but offset by a 180-degree phase difference. The selected frequency for these sine waves was 0.2 Hz, and the amplitude corresponded to an air pressure of 100 kPa, which was limited to positive values, as negative amplitudes were not utilized. The repetitive flexion and extension movements were quantified through the angular measurements of both the fingertips and roots, using 2D markers as reference points (Fig. 13). The measurements were made on a dummy hand model and on the actual subject's hand.

The final concept implementation test included various grasping tasks associated with a specific object. Balls, paper, and spoons were selected as objects corresponding to the three-point, tip, and lateral pinch. Depending on the object in question, pneumatic pressure patterns were pre-established, allowing the desired grasping mode to be executed via the GUI. During the tests, subjects wore a soft rehabilitation glove and initiated a reaching motion toward the target object with their fingers in a relaxed state. Subsequently, the task of object grasping was executed through GUI manipulation. Informed consent was obtained from the subjects before these measurements.

IV. RESULTS

A. CHARACTERIZATION OF FOLDABLE POUCH ACTUATOR

In terms of load-bearing capacity, FPAs demonstrated the ability to withstand forces up to 13.3 N without deviating

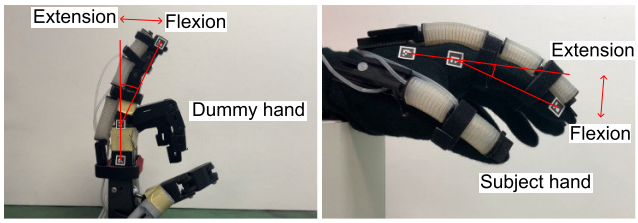

FIGURE 13. A dummy hand model and a subject's hand, both outfitted with a soft rehabilitation glove, were used. Repetitive flexion-extension movements were measured using 2D markers.

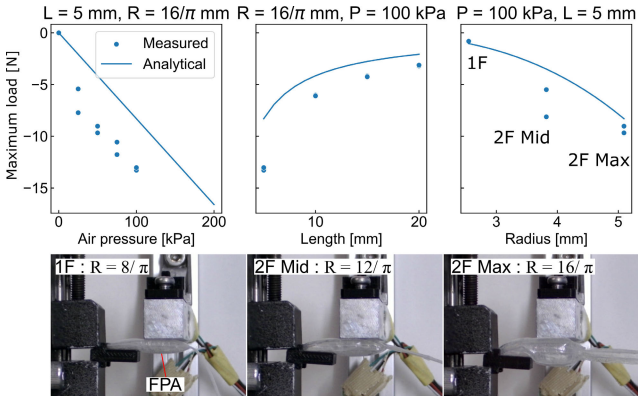

FIGURE 14. Measured maximum load and analysis results of FPAs. The three graphs in the upper half show the measured maximum load and analytical value from Equations 1 and 2 under each condition. The lower half shows behavior of each type of FPA being measured.

from a linear form, as depicted in Fig. 14. These empirically determined maximum loads aligned closely with the theoretical predictions (Equation 2). Consistent with the model, the maximum load exhibited direct proportionality to the air pressure and inverse proportionality to the actuator length. Moreover, upon pressurization and cylindrical expansion, the maximum load was found to be proportional to the cube of the actuator radius. This suggests that a folding structure with a radius twice as large would be expected to accommodate a maximum load eight times greater.

B. CHARACTERIZATION OF INTEGRATED ACTUATOR

The performance of the integrated actuator was characterized in both extension and flexion directions. When employing a 2F Max type actuator, the maximum achievable bending angle in the extension direction was found to be 26.2° (Fig. 15). The maximum bending angles of the 1F and 2F Mid types were lower than that of the 2F Max type at 14.7° and 16.5°, respectively (Table 2). Vibrations observed in the angle measurement curve were attributed to fluctuations caused by FPA chamber pressurization. As with the standalone FPA, the bending angle demonstrated proportionality to the applied air pressure. Additionally, the characteristics of the folding structure, notably the increase in radius upon expansion, had a significant impact on bending behavior in the extension direction.

Contrastingly, the maximum bending angle observed in the flexion direction using a 1F type actuator was 116.6°. The influence of variations in the folding structure on flexion was markedly less pronounced compared to extension. It is noteworthy that the integrated actuator equipped with the FPA achieved a greater maximum angle than the 95.2° achieved by a modular actuator lacking an FPA, as reported in prior research [18]. The bending behavior in flexion exhibited nonlinearity, a trait commonly observed in pneumatic and superelastic materials [23].

As presented in Fig. 15, the initial tip force in the extension direction, denoted by solid lines, commenced at approximately −2 N. This initial force was attributed to the inherent viscoelastic properties of the modular elastomeric actuator. Consequently, the maximum tip force achieved by the integrated actuator in the extension direction was measured to be 4.5 N using the 2F Max type. The integration of the folding structure also led to an enhancement of tip force in the extension direction.

Conversely, in the flexion direction, the maximum tip force was approximately 11.0 N when using a 2F Mid type actuator. Unlike the findings related to the bending angle, the impact of structural variations on tip force was less discernible in the flexion direction. Furthermore, the tip force results exhibited reduced nonlinearity, a deviation attributable to the specific experimental setup that minimized deformation caused by chamber expansion during force measurements.

Concerning the deflection behavior during simultaneous pressurization of both extension and flexion chambers, a consistent pattern was observed across the three different FPAs: an increase in the pressure within the extension chamber led to a decrease in deflection (Fig. 16). This suggests that the internal pressure of the extension chamber contributed positively to actuator stiffness. In contrast, for the 1F type integrated with an FPA, deflection increased when the pressure in the flexion chamber was escalated to 90 kPa. However, in the case of the 2F type, deflection behavior varied based on specific combinations of air pressures in both the extension and flexion chambers. This particular observation was noted when the air pressure in the extension chamber exceeded 140 kPa, while the air pressure in the bending chamber ranged between 30 and 70 kPa. Notably, this decrease in deflection was most pronounced when the air pressure in the extension chamber was 200 kPa and that in the bending chamber was 70 kPa. As the air pressure in the bending chamber increased, deflection exhibited different degrees of increase for the 2F Mid and Max types.

C. EVALUATION OF ACTUATORS WITH DUMMY FINGER

With regard to the ROM at the MCP joint, maximum flexion and extension values were measured to be 80.4° and -3.4° respectively when using the 2F Mid type actuator. As indicated in Fig. 17, the ROM for both extension and flexion demonstrated an almost linear relationship with applied air pressure. Although minor variations were observed in the joint extension ROM depending on the FPA

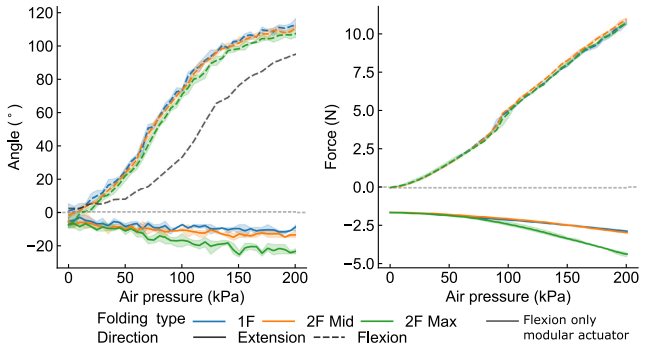

FIGURE 15. Results of integrated actuator characterization. From left to right: bending angle and tip force.

TABLE 2. Maximum bending angle and tip force of flexion-only and integrated actuators with different folding types.

Folding type of FPA	Bending angle (°)		Tip force (N)	
	E	F	E	F
Flexion only modular actuator	-	95.2	-	-
1F	14.7	116.6	2.9	10.9
2F Mid	16.5	112.9	3.0	11
2F Max	26.2	109.7	4.5	10.7

E extension, F flexion, '-' not available

structure, these differences were rendered insignificant at an air pressure of 200 kPa. Consequently, the incorporation of the folding structure into the actuator did not substantially influence the ROM in joint extension.

The data presented in the right half of Fig. 17 elucidate the joint flexion and extension torques at varying initial joint angles. The flexion torque attained its peak value at an initial angle of 0° and subsequently diminished as the initial angle increased. Analogous to the findings on ROM, the FPA did not exert a substantial influence on flexion torque. In contrast, the 2F Max FPA registered the highest extension torque across all initial angles, with the exception of 0°. Furthermore, the extension torque displayed an initial increase from 0° to between 15° and 45°, after which it declined to zero at 90°.

D. SOFT REHABILITATION GLOVE PERFORMANCE

As shown in Fig. 18, the angle represents the degree of finger flexion; a greater angle signifies increased flexion, while a smaller angle indicates enhanced extension during the grasping action. Consequently, it is advantageous for the angle waveform to conform to the control signal of the air pressure in the flexion chamber. The observations confirm that the angle closely approximates this ideal behavior. This indicates the proposed actuator can distinguish between flexion and extension to support motion. Because of the difference in initial angles and joint stiffness between the dummy hand model and the subject's hand, overall, the angles measured on the subject's hand tended to be smaller, but the responsiveness did not change significantly.

Finally, Fig. 19 depicts the results of the grasping tests, revealing the successful grasping of various objects such as balls, papers, and spoons with glove assistance.

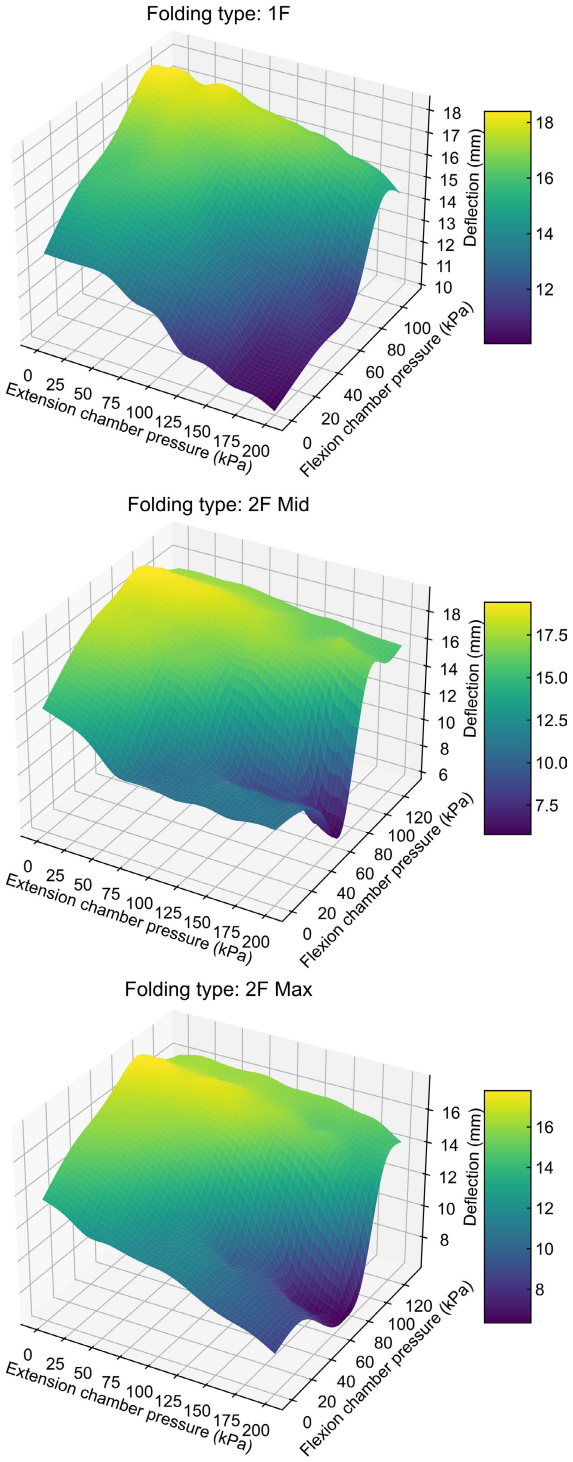

FIGURE 16. Deflection results during co-pressurization of chambers of both extension and flexion actuators.

V. DISCUSSION

A. CHARACTERIZATION OF FOLDABLE POUCH ACTUATOR

The implemented FPA exhibited characteristics largely concordant with the theoretical models also discussed in pertinent literature (Equation 2). Specifically, the increased radius during expansion substantially contributed to increased

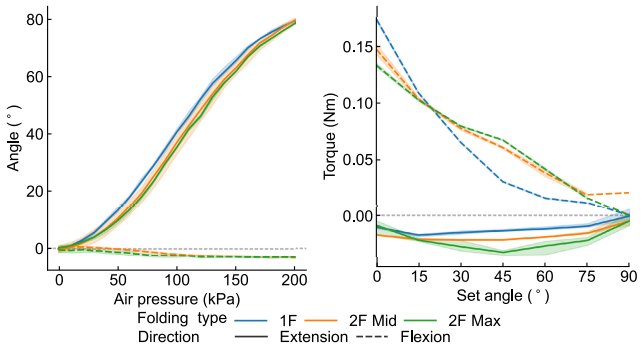

FIGURE 17. Evaluation results of integrated actuators on dummy fingers, ROM and torque in flexion and extension of MCP joints.

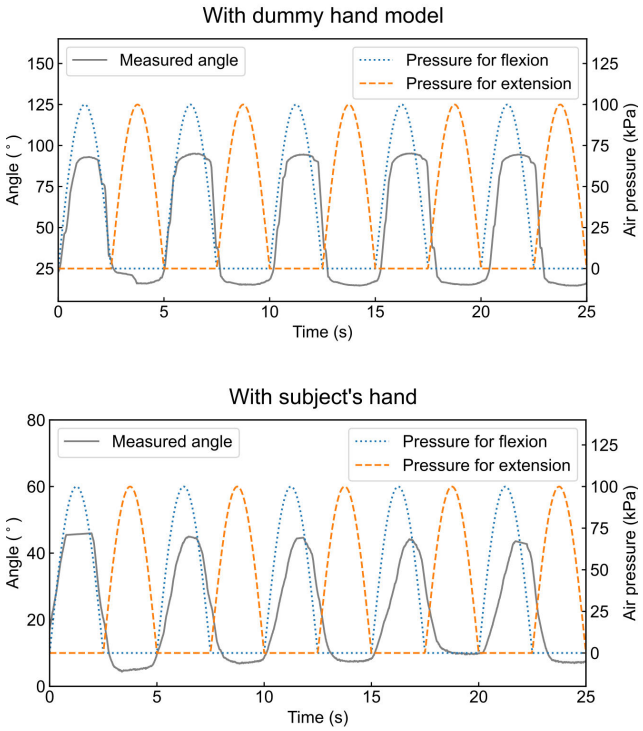

FIGURE 18. The tracking performance of the soft rehabilitation glove, demonstrated on both a dummy hand model and a subject's hand, showcases the control signal and angle tracking capabilities.

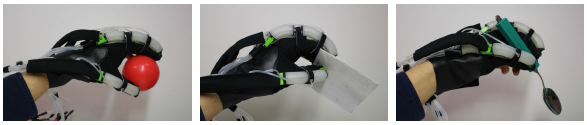

FIGURE 19. Grasping results, from left to right: ball, paper, and spoon.

actuator stiffness, corroborating the model's predictions. Such enhanced stiffness is particularly beneficial in confined spaces, such as those between finger joints. These findings are in agreement with research that employed standard inflatable tubes in reel-type actuators [35]. Adapted for the first time for applications in hand rehabilitation, especially for aiding in extension, this model has demonstrated a degree of reliability in terms of the forces generated. Consequently, the design of the FPA can be fine-tuned to cater to the specific joint conditions of the patient.

Due to constraints imposed by the fabrication equipment and the handmade nature of the system, this study was limited to the realization of two-fold folding structures. Nonetheless, the adoption of more sophisticated and automated fabrication techniques could facilitate an increase in both the radius of expansion and extension torque. During this process, meticulous attention must be accorded to the production phase, as an excessive enlargement in the radius of expansion could result in unanticipated interactions with the integrated actuator. A minor deviation was noted between the empirical data and the theoretical model. This disparity could be ascribed to elements not accounted for in the model, such as deformations introduced by the folding structures or the effects of sealed ends. These elements prevent the attainment of a perfectly circular shape upon expansion, suggesting that an elliptical model may offer a more accurate approximation.

B. CHARACTERIZATION OF INTEGRATED ACTUATOR

The characterization results for the integrated actuator, when considered independently, largely conform to the trends hypothesized in our preceding work and the models developed for the FPA. The bending angles in the flexural direction primarily originated from the modular actuator, although the inclusion of an FPA at the bottom surface engendered greater bending angles compared to conventional modular actuators. The FPA attenuated the elongation at the base of the existing modular actuator. Consequently, from the perspective of energy conservation, the inflow of pneumatic energy was exclusively harnessed for bending action, thereby yielding superior bending angles relative to traditional actuators. However, the magnitude of this variation was modestly influenced by the number of folds in the FPA. Specifically, an increase in the number of folds culminated in a reduced bending angle. Despite the FPA's composition of an exceedingly thin film, a higher number of folds incrementally thickened the bottom surface. It logically follows that an augmented thickness would escalate bending stiffness, thereby marginally diminishing bending. Although the impact of the number of folds was negligible in relation to the overall bending angle due to the limited range of folds tested, this factor warrants consideration for future research involving an increased number of folds.

The bending angle in the extension direction was influenced by the expansion of the FPA located at the base of the modular actuator. This expansion enabled the actuator to bend in the extension direction. Notably, the resultant angle in this direction exhibited a positive correlation with the number of folds in the folding structure. An increase in the number of folds expanded the cross-sectional area during pneumatic activation, thereby elevating the level of deformation. Consequently, the enhanced deformation at the base led to increased extension.

This rationale can be extended to the analysis of tip forces as well. The forces in the flexural direction demonstrated a comparable trend across all types of actuators, with only minor discrepancies. Contrary to the results for bending angles, the variation in the tip force data was less pronounced and the resulting curves exhibited greater linearity. This discrepancy may be attributed to the measurement methodology, as the setup for measuring tip force imposed additional constraints that largely restricted deformations other than those directly affecting the tip force.

With regard to the deflection behavior under applied load, a consistent trend emerged: deflection diminished as pressure was increased in the extension chamber. This behavior signified an increase in stiffness in the extension chamber as a function of air pressure, a finding consistent with both the theoretical model and the empirical characterization of the FPA. Furthermore, compared to conventional preloading of the flexion chamber only for extension, pressurizing the FPA reduces deflection in almost all situations, providing an advantage with respect to stiffness generation for extension support. Nonetheless, the behavior in the deflection displayed sensitivity to the presence or absence of a folding structure. Specifically, the 1F type actuator, which lacked a folding structure, exhibited an increase in deflection as pressure was applied to the flexion chamber.

In contrast, the 2F type featuring a folding structure initially exhibited a decline in deflection upon flexion chamber pressurization, followed by an increase in deflection, mirroring the behavior of the 1F type. This phenomenon is believed to arise because the two chambers function in a manner akin to antagonistic muscles when activated, thereby augmenting stiffness. Consequently, the 1F type, characterized by its inherently lower radius of expansion and, thus, reduced stiffness, was less capable of counteracting the forces generated within the flexion chamber. However, the 2F type possessed sufficient stiffness to counterbalance the forces within the flexion chamber, particularly when subjected to a specific combination of air pressures. Notably, this enhancement in stiffness was most pronounced when the air pressure in the flexion chamber reached 70 kPa and that in the extension chamber was 200 kPa. Furthermore, the extent of this peak deflection reduction varied slightly with the type of folding structure: 2F Max, i.e., FPA with a larger radius at expansion, produced a state of deflection reduction that was antagonistic to the flexion chamber over a wider range than 2F Mid. This shows the optimal conditions for achieving high stiffness differ between folding structures. Such a feature enables the actuator to deliver specific stiffness levels to the wearer and holds promise for applications beyond rehabilitation assistance, including stiffness and pressure feedback systems. To the best of our knowledge, this study is the first to report on such capabilities in joint-specific modular actuators. Nevertheless, to ascertain the specific stiffness characteristics, a more elaborate mechanistic model of the antagonistic actuator system is necessary.

C. EVALUATION OF ACTUATORS WITH DUMMY FINGER

The ROM observed in the MCP joint of the dummy finger equipped with the integrated actuator displayed a trend congruent with that observed in the isolated actuator's bending angle measurements. The applied air pressure led to deformation of the actuator, either in the direction of flexion or extension, thereby facilitating the bending motion of the finger joint. Contrary to the observations made with the standalone actuator, the variation in ROM was minimized when the actuator was affixed to the dummy finger, thereby suppressing vibrational artifacts during the measurement process. Although the flexion angle demonstrated some dependency on the type of FPA employed, the angles converged to a similar value at an air pressure of 200 kPa. This convergence may be attributed to the intrinsic maximum ROM of the dummy fingers, beyond which no further bending occurred. Therefore, the measurements likely stabilized around this upper limit.

In the extension direction, an increase in the expansion radius of the FPA was hypothesized to result in greater bending angles. However, the observed bending angles exhibited minimal variation across different FPA types. This lack of variation can be ascribed to the geometrical constraints imposed by the dummy fingers. Designed with a rectangular shape for ease of actuator mounting and experimental repeatability, these dummy fingers limited the expansion of the actuator's bottom surface to the upper surface of the dummy finger. Consequently, the extent of deformation in the extension direction remained relatively consistent among the various types of FPA. Nonetheless, these findings may have limited applicability in actual rehabilitation settings, where the natural ROM for DIP and PIP joints in the extension direction is generally 0°. Exceeding this limit could potentially result in damage to the joint tissue.

The extension torque exerted on the MCP joints was contingent upon the pre-established joint angle at the time of measurement.

Furthermore, the data indicated that FPA types with larger radii upon inflation generated greater extension torque, a finding that is consistent with the standalone characterization of the FPAs. Notably, the extension torque varied as a function of angle and was influenced by the specific type of FPA utilized. While extension torque generally diminished at 0° or 90°, the angle at which the peak torque was achieved differed among the various FPA types. Type 1F, characterized by the smallest radius of expansion, reached its apex at approximately 15°. Conversely, as the radius of expansion increased with different FPA types, the angle corresponding to maximum extension torque also rose. Although this trend may initially appear paradoxical, it aligns with prior research examining the resilience of inflatable tubes when bent [36]. Such tubes, when bent past a particular angle, tend to exhibit wrinkling at the bend, thereby diminishing the restoring force. It is postulated that a similar phenomenon occurred

TABLE 3. Functional comparison of soft actuators for hand rehabilitation assistance.

Group	Actuator Type	Assisted Motion	Individual Joints Assist	Input Air Pressure	Bending Angle of Actuator	E / F force of Actuator	E / F torque w/ or w/o Finger	
Yap et al. [31]	WF	E/F	N	70 kPa	-	- / 14 N	0.31 Nm / -	(only actuator)
Yun et al. [15]	M	F	Y	300 kPa	*0 $\sim$ 90°	-	- / *0.17 Nm	(with finger)
Cappello et al. [32]	WF	E/F	N	172 kPa	-	-	0.18 / 0.15 Nm	(only actuator)
Hu et al., 2020 [16]	M	E/F	Y	70 kPa	-	4.6 / 1.9 N	-	
Kokubu et al. [18]	M	F	Y	200 kPa	0 $\sim$ 95.2°	- / 13.2 N	- / 0.17 Nm	(with finger)
This study	M	E/F	Y	200 kPa	$-26.2 \sim 116.6°$	4.5 / 11 N	0.04 / 0.17 Nm	(with finger)

E extension, F flexion, WF whole-finger, M modular, '-' value not reported, '$*$' estimated value from figure

during the extension torque measurements on the MCP joint, given that the FPA was purposely placed in a bent state for these assessments. A reduction in extension torque at around 90° could be disadvantageous for patients requiring rehabilitation of contracted joints. One possible remediation could be the selection of materials that minimize wrinkling in the flexed state. However, opting for more rigid films warrants caution, as such materials could obstruct actuator movement in the flexion direction.

In summary, the evaluation of the dummy finger actuators demonstrated that the capacity to extend individual joints could be incorporated without negatively impacting the flexion capabilities of pre-existing actuators. This conclusion was substantiated by the comparison of critical performance metrics—such as bending angle, force, and torque—with those of soft actuators described in pertinent literature.

The comparative analysis of soft actuators presented in Table 3 highlights several key distinctions. Among these, the actuator proposed in this study exhibited superior flexion angles compared to those documented in related works and uniquely offered the capability for individual joint extension angles. The extension force of the proposed actuator is on par with the bellows-based actuator reported by Hu et al. [16], whereas its flexion force is approximately sixfold greater.

However, the extension torque of the proposed actuator lagged behind those reported by Yap et al. [31] and Cappelo et al. [32], both of which were designed to facilitate extension for the entire finger. This disparity can primarily be attributed to differences in actuator design and measurement methodologies. Actuators with higher torque values were generally engineered to encompass the full finger and thus are not directly comparable to modular types. Moreover, a degree of interaction and energy loss may occur when assessing the actuator in isolation as opposed to in conjunction with fingers.

For the proposed actuator design, three modular units are required to interface with a single finger. Based on the data provided in Table 3, the aggregate extension torque necessary to actuate a single finger is estimated at 0.12 Nm, obtained by tripling the individual actuator values. Although this figure remains lower than those cited in certain related studies, it nevertheless offers a stable performance, particularly when viewed in conjunction with its flexion torque capabilities. The torque deficit could potentially be mitigated through the incorporation of additional folding structures.

In summary, the proposed actuator design presents a noteworthy advancement in the field of soft actuators. The main innovations detailed in this paper, which distinguish it from the current state-of-the-art in soft robotics, soft actuators, hand rehabilitation, and related fields, are as follows:

- The development of a FPA, conceptualized through mathematical modeling, to deliver high efficiency within constrained spatial configurations. This innovation allows for the construction of compact, high-performance soft actuators.
- Integrating a FPA fabricated from sheet material with a modular actuator made of elastomer materials. This combination enables the creation of soft actuators capable of various motion mechanisms, enhancing their versatility and broadening their application spectrum.
- A novel architectural design that facilitates the seamless integration of these components, avoiding mutual interference and supporting motion in both flexion and extension of joints. This design is particularly advantageous for offering improved assistance in hand rehabilitation, among other potential applications.

D. SOFT REHABILITATION GLOVE PERFORMANCE

Grasping tests utilizing a glove fitted on a healthy individual yielded encouraging results, despite the glove's limitation to three fingers to minimize complexities related to pneumatic tubing and control systems. The tests demonstrated that the glove could successfully facilitate grasping postures through the coordinated flexion and extension of individual finger joints, and achieve fixation at specific angles. These results affirm that the proposed glove design can integrate extension capabilities without undermining the flexion functionality offered by the existing actuator.

During the evaluation of grasping motion, the glove was generally successful in tracking the 0.2 Hz cyclic control signals. However, minor anomalies were observed: a slight variability in the amplitude of extension movements and a minor temporal delay. These issues were attributed to two factors—partial obstruction of pneumatic tubes connected to the extension chambers, and inflation challenges stemming from fabrication errors. In the context of rehabilitation, the observed delay of approximately 0.8 seconds is unlikely to be clinically problematic, as premature actuation could risk injuring the patient's hand tissues.

Notwithstanding its current limitations, the glove shows promise for application in hand training programs, contingent on advancements in manufacturing techniques. The

tasks used for testing, though elementary, are highly relevant for rehabilitation training aimed at enhancing the flexibility of hand and finger joints. Most conventional rehabilitation gloves are not engineered to actively support extension movements, making them suboptimal for executing repeated simple grasping motions. Additionally, the effectiveness of gloves designed for whole-finger extension in accommodating the varying stiffness across joints remains uncertain.

In contrast, the actuator-based glove proposed in this study is equipped to facilitate bidirectional flexion-extension movements across individual joints. This capability positions it as a promising alternative to traditional in-person rehabilitation methods, specifically for patients requiring joint-specific intervention.

VI. CONCLUSION

In this study, a FPA designed for joint-specific extension support was introduced and amalgamated into an extant modular soft actuator to enable dynamic support for joint-specific flexion and extension. Initially, the FPA underwent stand-alone characterization, demonstrating substantial concordance with the computational model under maximum load conditions and achieving a maximum load force of 13.3 N for extension support. Subsequent experimental characterizations of the integrated actuator, along with evaluations using a synthetic finger model, affirmed its basic capabilities for flexion-extension support, achieving 0.17 Nm for individual joint flexion and 0.12 Nm for overall finger extension. To substantiate the applicability of the integrated actuator, a glove equipped with this device underwent flexion/extension movement tests when worn by a subject. These tests confirmed the glove's viability for facilitating coordinated flexion and extension of finger joints. Future investigations will aim to rectify existing shortcomings, such as manufacturing inaccuracies that impede the inflation of extension chambers, and the complications arising from the increased degrees of freedom in control systems. This refinement is expected to further optimize the actuator for more specialized applications, particularly in the realm of joint-specific rehabilitation.

ACKNOWLEDGMENT

The authors would like to thank Yuxi Lu and Zhongchao Zhou for providing insights into the design of the soft actuator. They also would like to thank Editage (www.editage.jp) for English language editing.

REFERENCES

[1] B. Mosadegh, P. Polygerinos, C. Keplinger, S. Wennstedt, R. F. Shepherd, U. Gupta, J. Shim, K. Bertoldi, C. J. Walsh, and G. M. Whitesides, "Pneumatic networks for soft robotics that actuate rapidly," *Adv. Funct. Mater.*, vol. 24, no. 15, pp. 2163–2170, Apr. 2014.

[2] P. Polygerinos, K. C. Galloway, E. Savage, M. Herman, K. O. Donnell, and C. J. Walsh, "Soft robotic glove for hand rehabilitation and task specific training," in *Proc. IEEE Int. Conf. Robot. Autom. (ICRA)*, May 2015, pp. 2913–2919.

[3] X. Li, Y. Hao, J. Zhang, C. Wang, D. Li, and J. Zhang, "Design, modeling and experiments of a variable stiffness soft robotic glove for stroke patients with clenched fist deformity," *IEEE Robot. Autom. Lett.*, vol. 8, no. 7, pp. 4044–4051, Jul. 2023.

[4] S. Kokubu, P. E. T. Vinocour, and W. Yu, "Development and evaluation of fiber reinforced modular soft actuators and an individualized soft rehabilitation glove," in *Intelligent Autonomous Systems 17* (Lecture Notes in Networks and Systems), vol. 577. Amsterdam, The Netherlands: Elsevier, 2023, pp. 139–152.

[5] K. C. Galloway, P. Polygerinos, C. J. Walsh, and R. J. Wood, "Mechanically programmable bend radius for fiber-reinforced soft actuators," in *Proc. 16th Int. Conf. Adv. Robot. (ICAR)*, Nov. 2013, pp. 1–6.

[6] T. Tarvainen, J. Fernandez-Vargas, and W. Yu, "New layouts of fiber reinforcements to enable full finger motion assist with pneumatic multi-chamber elastomer actuators," *Actuators*, vol. 7, no. 2, p. 31, Jun. 2018.

[7] Y. Wang, S. Kokubu, S. Huang, Y.-H. Hsueh, and W. Yu, "Towards an extensive thumb assist: A comparison between whole-finger and modular types of soft pneumatic actuators," *Appl. Sci.*, vol. 12, no. 8, p. 3735, Apr. 2022.

[8] F. Connolly, C. J. Walsh, and K. Bertoldi, "Automatic design of fiber-reinforced soft actuators for trajectory matching," *Proc. Nat. Acad. Sci. USA*, vol. 114, pp. 51–56, Jan. 2017.

[9] Z. Chen, A. Zou, Z. Qin, X. Han, T. Li, and S. Liu, "Modeling and fabrication of soft actuators based on fiber-reinforced elastomeric enclosures," *Actuators*, vol. 10, no. 6, p. 127, Jun. 2021.

[10] G. Yang, E. P. McGlinn, and K. C. Chung, "Management of the stiff finger: Evidence and outcomes," *Clinics Plastic Surg.*, vol. 41, no. 3, pp. 501–512, 2014.

[11] E. F. Elaine, A. P. Cynthia, and W. S. James, *Hand Splinting: Principles and Methods Japanese Translation*. Maryland Heights, MO, USA: C. V. Mosby Company, 1981.

[12] R. M. Patterson, C. W. Stegink Jansen, H. A. Hogan, and M. D. Nassif, "Material properties of thera-band tubing," *Phys. Therapy*, vol. 81, no. 8, pp. 1437–1445, Aug. 2001.

[13] Z. Q. Tang, H. L. Heung, K. Y. Tong, and Z. Li, "Model-based online learning and adaptive control for a 'human-wearable soft robot' integrated system," *Int. J. Robot. Res.*, vol. 40, pp. 256–276, Jan. 2021.

[14] Q. Peng, H.-S. Park, P. Shah, N. Wilson, Y. Ren, Y.-N. Wu, J. Liu, D. J. Gaebler-Spira, and L.-Q. Zhang, "Quantitative evaluations of ankle spasticity and stiffness in neurological disorders using manual spasticity evaluator," *J. Rehabil. Res. Develop.*, vol. 48, no. 4, p. 473, 2011.

[15] S.-S. Yun, B. B. Kang, and K.-J. Cho, "Exo-glove PM: An easily customizable modularized pneumatic assistive glove," *IEEE Robot. Autom. Lett.*, vol. 2, no. 3, pp. 1725–1732, Jul. 2017.

[16] D. Hu, J. Zhang, Y. Yang, Q. Li, D. Li, and J. Hong, "A novel soft robotic glove with positive-negative pneumatic actuator for hand rehabilitation," in *Proc. IEEE/ASME Int. Conf. Adv. Intell. Mechatronics (AIM)*, Jul. 2020, pp. 1840–1847.

[17] S. Kokubu and W. Yu, "Developing a hybrid soft mechanism for assisting individualized flexion and extension of finger joints," in *Proc. 42nd Annu. Int. Conf. IEEE Eng. Med. Biol. Soc. (EMBC)*, Jul. 2020, pp. 4873–4877.

[18] S. Kokubu, Y. Wang, P. E. Tortós Vinocour, Y. Lu, S. Huang, R. Nishimura, Y.-H. Hsueh, and W. Yu, "Evaluation of fiber-reinforced modular soft actuators for individualized soft rehabilitation gloves," *Actuators*, vol. 11, no. 3, p. 84, Mar. 2022.

[19] P. Polygerinos, Z. Wang, K. C. Galloway, R. J. Wood, and C. J. Walsh, "Soft robotic glove for combined assistance and at-home rehabilitation," *Robot. Auto. Syst.*, vol. 73, pp. 135–143, Nov. 2015.

[20] H. Kai. Yap, B. W. K. Ang, J. Hoon. Lim, J. C. H. Goh, and C.-H. Yeow, "A fabric-regulated soft robotic glove with user intent detection using EMG and RFID for hand assistive application," in *Proc. IEEE Int. Conf. Robot. Autom. (ICRA)*, May 2016, pp. 3537–3542.

[21] H. K. Yap, N. Kamaldin, J. H. Lim, F. A. Nasrallah, J. C. H. Goh, and C.-H. Yeow, "A magnetic resonance compatible soft wearable robotic glove for hand rehabilitation and brain imaging," *IEEE Trans. Neural Syst. Rehabil. Eng.*, vol. 25, no. 6, pp. 782–793, Jun. 2017.

[22] H. K. Yap, J. H. Lim, F. Nasrallah, and C.-H. Yeow, "Design and preliminary feasibility study of a soft robotic glove for hand function assistance in stroke survivors," *Frontiers Neurosci.*, vol. 11, pp. 1–14, Oct. 2017.

[23] K. Shiota, S. Kokubu, T. V. J. Tarvainen, M. Sekine, K. Kita, S. Y. Huang, and W. Yu, "Enhanced kapandji test evaluation of a soft robotic thumb rehabilitation device by developing a fiber-reinforced elastomer-actuator based 5-digit assist system," *Robot. Auto. Syst.*, vol. 111, pp. 20–30, Jan. 2019.

[24] Y. Han, Q. Xu, and F. Wu, "Design of wearable hand rehabilitation glove with bionic fiber-reinforced actuator," *IEEE J. Transl. Eng. Health Med.*, vol. 10, pp. 1–10, 2022.
[25] K. Ma, Z. Jiang, S. Gao, X. Cao, and F. Xu, "Design and analysis of fiber-reinforced soft actuators for wearable hand rehabilitation device," *IEEE Robot. Autom. Lett.*, vol. 7, no. 3, pp. 6115–6122, Jul. 2022.
[26] Y. Wang, S. Kokubu, Z. Zhou, X. Guo, Y.-H. Hsueh, and W. Yu, "Designing soft pneumatic actuators for thumb movements," *IEEE Robot. Autom. Lett.*, vol. 6, no. 4, pp. 8450–8457, Oct. 2021.
[27] R. Niiyama, D. Rus, and S. Kim, "Pouch motors: Printable/inflatable soft actuators for robotics," in *Proc. IEEE Int. Conf. Robot. Autom. (ICRA)*, May 2014, pp. 6332–6337.
[28] M. A. Robertson, O. C. Kara, and J. Paik, "Soft pneumatic actuator-driven origami-inspired modular robotic 'pneumagami,'" *Int. J. Robot. Res.*, vol. 40, no. 1, pp. 72–85, Jan. 2021.
[29] J. H. Jang, B. Jamil, Y. Moon, A. Coutinho, G. Park, and H. Rodrigue, "Design of gusseted pouch motors for improved soft pneumatic actuation," *IEEE/ASME Trans. Mechatronics*, vol. 28, pp. 3053–3063, Dec. 2023.
[30] J. A. Main, S. W. Peterson, and A. M. Strauss, "Load-deflection behavior of space-based inflatable fabric beams," *J. Aerosp. Eng.*, vol. 7, no. 2, pp. 225–238, Apr. 1994.
[31] H. K. Yap, P. M. Khin, T. H. Koh, Y. Sun, X. Liang, J. H. Lim, and C.-H. Yeow, "A fully fabric-based bidirectional soft robotic glove for assistance and rehabilitation of hand impaired patients," *IEEE Robot. Autom. Lett.*, vol. 2, no. 3, pp. 1383–1390, Jul. 2017.
[32] L. Cappello, K. C. Galloway, S. Sanan, D. A. Wagner, R. Granberry, S. Engelhardt, F. L. Haufe, J. D. Peisner, and C. J. Walsh, "Exploiting textile mechanical anisotropy for fabric-based pneumatic actuators," *Soft Robot.*, vol. 5, no. 5, pp. 662–674, Oct. 2018.
[33] L. Ge, F. Chen, D. Wang, Y. Zhang, D. Han, T. Wang, and G. Gu, "Design, modeling, and evaluation of fabric-based pneumatic actuators for soft wearable assistive gloves," *Soft Robot.*, vol. 7, no. 5, pp. 583–596, Oct. 2020.
[34] *Human Hand Dimensions Data for Ergonomic Design 2010*, Res. Inst. Human Eng. Quality Life, Osaka, Japan, 2010.
[35] Z. M. Hammond, N. S. Usevitch, E. W. Hawkes, and S. Follmer, "Pneumatic reel actuator: Design, modeling, and implementation," in *Proc. IEEE Int. Conf. Robot. Autom. (ICRA)*, May 2017, pp. 626–633.
[36] J. Wei, H. Ding, Y. Chai, A. Eriksson, and H. Tan, "Quasi-static folding and deployment of rigidizable inflatable beams," *Int. J. Solids Struct.*, vol. 232, Dec. 2021, Art. no. 111063.

SHOTA KOKUBU received the B.Eng. and M.Eng. degrees in medical engineering from Chiba University, Japan, in 2019 and 2021, respectively. He is currently pursuing the Ph.D. degree with the Department of Medical Engineering, Graduate School of Science and Engineering, Chiba University. His research interests include soft rehabilitation devices and human-rehabilitation device interface design and construction.

PABLO E. TORTÓS VINOCOUR received the B.Eng. degree in mechatronics engineering from Costa Rica Institute of Technology, Costa Rica, in 2019, and the M.Eng. degree in medical engineering from Chiba University, Japan, in 2022. He is currently pursuing the Ph.D. degree with the Department of Medical Engineering, Graduate School of Science and Engineering, Chiba University. His research interests include soft robotics, rehabilitation robotics, finite element modeling, and biomechanical design.

WENWEI YU (Member, IEEE) received the B.Eng. and M.Eng. degrees from Shanghai Jiao Tong University, in 1989 and 1992, respectively, and the Ph.D. degree in system information engineering and the Ph.D. degree in rehabilitation medical science from Hokkaido University, Japan, in 1997 and 2003, respectively. He was an Assistant Professor with the Department of System Information Engineering, School of Engineering, Hokkaido University, from 1999 to 2003. In 2003, he was an Exchange Research Fellow with the Center for Neuroscience, University of Alberta, Canada, supported by the Researcher Exchange Program, Japanese Society for the Promotion of Science (JSPS). Since 2004, he has been an Associate Professor with the Department of Medical System Engineering, School of Engineering, Chiba University, Japan. Since 2006, he has been with the AI Laboratory, Zurich University, Switzerland, as a Visiting Professor supported by JSPS. He has been a Professor, since 2009. He has authored and coauthored more than 150 articles in refereed journals and book chapters, and more than 170 international conference papers. His research interests include neuro-prosthetics, rehabilitation robotics, motor control and biomedical signal processing. He is a member of the Robot Society of Japan (RSJ) and Japanese Society for Medical and Biological Engineering (JSMB).